This article has been accepted for publication in a future issue of this journal, but has not been fully edited. Content may change prior to final publication. Citation information: DOI 10.1109/TIA.2018.2869880, IEEE Transactions on Industry Applications

Single Stage SECS Interfaced with Grid Using ISOGI-FLL Based Control Algorithm

Priyank Shah, *Member, IEEE,* Ikhlaq Hussain, *Member, IEEE* and Bhim Singh, *Fellow, IEEE*

***Abstract*-This paper proposes an Improved Second-Order Generalized Integrator with Frequency Locked Loop (ISOGI-FLL) based control scheme for grid-connected solar Photovoltaic (PV) array fed Voltage Source Converter (VSC) to mitigate the power quality (PQ) problems. The steepest descent algorithm based Maximum Power Point Tracking (MPPT) is used to achieve the crest power from a solar PV array to improve Solar Power Generation (SPG) into the grid as well as to maintain DC bus voltage of the VSC. The ISOGI-FLL based control scheme is very effective for grid currents balancing, harmonics mitigation, at a variation of solar power generation and unity power factor operation. Simulated results are demonstrated using MATLAB/Simulink for load unbalancing and variation in solar insolation. The effectiveness of the proposed algorithm is demonstrated based on comparative performance with conventional algorithms. Test results of a developed prototype, show satisfactory performance for different operating conditions like grid currents balancing, Photovoltaic-Distribution Static Compensator (PV-DSTATCOM) mode, DSTATCOM-PV mode at variable solar insolation. Moreover, total harmonic distortions of grid voltages-currents, are achieved within the limit of the IEEE-519 standard.**

Keywords- ISOGI-FLL, MPPT, Power Quality, Solar Photovoltaic and VSC.

I. INTRODUCTION

In India, a major part of electricity (68%) is produced by fossil fuels like coal and oil [1-2]. The greenhouse gases are produced from fossil fuel of power plants generation and that affects the environment [1]. Due to demand for large peak power, high import dependence (oil and increasingly coal) and energy inadequacy, indicate serious trouble related to energy security. There should be a balance between energy production and energy consumption. Therefore, domestic energy generation must be initiated in the distribution network by using rooftop Photovoltaic (PV) array for production of green energy to mitigate the environmental changes. Therefore, usages of rooftop PV array, are booming in small-scale application [3]. The Power Quality (PQ) issues in the grid, are predominant due to nonlinear loads in the distribution network. The power quality of grid is degraded due to nonlinear loads, which draw reactive power at Point of Common Coupling (PCC) like variable speed drives, Uninterruptible Power Supplies (UPS), motor drives, arc furnaces and residential loads etc.

Various configurations for the grid interfaced PV connected Voltage Source Converter (VSC) are proposed in [4]. The loss analysis for single-stage and two-stage Solar Energy Conversion Systems (SECSs), is demonstrated in the literature [5]. The single stage SECS has certain advantages over double stage SECS such as reduced complexity, reduced numbers of components (capacitor, diode etc.) and higher efficiency.

The PQ of the grid is degraded as, nonlinear loads such as computers, printers, lamps, arc furnaces, heavy rectifiers, UPS and variable frequency drives etc. are commonly connected at PCC [6]. The challenges in PQ improvement of the grid using renewable energy sources, are described in [7]. Javadi *et al.* [8] have proposed abc-dq transformation based multi-functional algorithm for zero voltage regulation, load balancing, reactive power compensation and noise elimination. The transformation-based control scheme has poor dynamic performance under varying operating condition. The current in direct axis contains second harmonic oscillation under unbalancing in load side network. The Least Mean Fourth (LMF) control algorithm [9] has been presented to make phase independent operation of the amplitude of the fundamental load current for PQ enhancement of the distribution grid. The LMF technique has inferior steady-state convergence rate due to fourth order optimization. The Model Predictive Control (MPC) based control scheme is presented in [10] for the PQ enhancement of the single phase system. The MPC has high memory and computation burden. The notch filter based algorithm is presented for the integration of distributed resources with the grid. The Phase Locked Loop (PLL) less technique [11] has poor DC component and harmonics elimination abilities. The performance of the system is affected, when load currents contain DC offset component. The Lyapunov function with sliding mode based control algorithm, is presented in the literature [12] for PQ enhancement of the distribution grid. The sliding mode control provides the hard switching to the converter, which leads to reducing the lifetime of the converter. The Kalman filter based technique is presented in [13], for grid-connected solar energy conversion system. The Kalman filter based algorithm has high computational burden, increased memory requirement, and high complexity. The parameters adjustment of Kalman filter is difficult and very sensitive under variation of system parameters. The Least Square (LS) based control scheme is presented in the literature [14], to extract fundamental load component. However, the accuracy of LS algorithm is disputable under variation of the system frequency.

Manuscript received Nov 23, 2017; revised March 20, 2017, May 15, 2018; accepted August 28, 2018. This work was supported by Department of Science and Technology, Government of India project under Grant RP03391 and J. C. Bose Fellowship under Grant RP03128. Paper no. 2017-SECSC-1361. *(Corresponding author: Priyank Shah.)*

Priyank Shah and Bhim Singh are with the Department of Electrical Engineering, Indian Institute of Technology Delhi, New Delhi, India (e-mail: p4priyank1504@gmail.com and bsingh@ee.iitd.ac.in).

Ikhlaq Hussain is with the Department of Electrical Engineering, Institute of Technology, University of Kashmir, Srinagar, J&K, India (e-mail: ikhlaqiitd@gmail.com).

This article has been accepted for publication in a future issue of this journal, but has not been fully edited. Content may change prior to final publication. Citation information: DOI 10.1109/TIA.2018.2869880, IEEE Transactions on Industry Applications

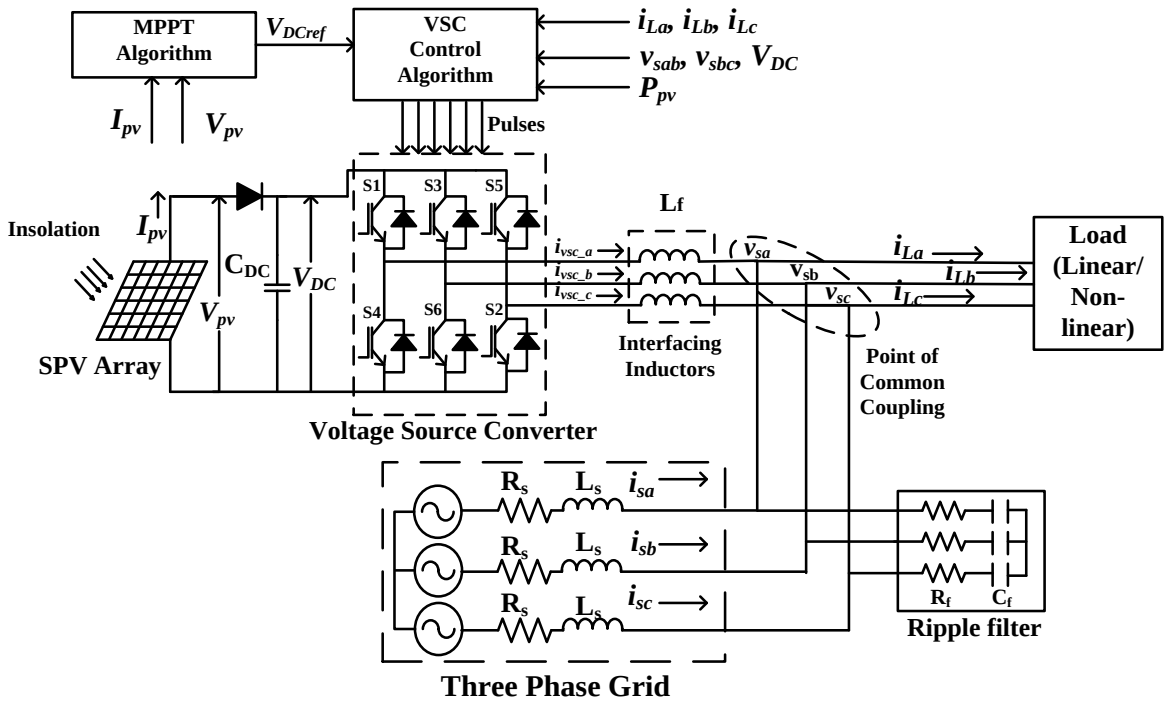

Fig.1 Schematic diagram of a presented system

The utility interactive inverters are described in the literature [15]. A multifarious control scheme is presented in [16], for shunt active power filter in the distribution network. This control algorithm lacks the grid currents balancing features. The neural network based control algorithms [17-18] have poor dynamic performance under unbalancing in load side network. The SECS performance is affected due to poor magnitude extraction abilities of the single layer neural network technique. The neural network algorithm requires expertise to train data. The behaviour of the system is influenced as it is unable to eliminate DC offset component from the load current.

The adaptive filter based control techniques such as Least Mean Square (LMS) [19], least logarithmic absolute difference [20], are presented for PQ enhancement of the distribution grid. The LMS algorithm has poor convergence rate with respect to LMF technique. The LMS algorithm has a high mean square error while estimating the magnitude of the fundamental load current. The back propagation technique has high complexity while designing a number of layers and training the data. Moreover, the performance of the system using an adaptive filter based control scheme [9, 19-20], is disputable under the presence of DC offset in load current and weak grid scenarios. The stability of system under weak grid scenario is analyzed in the literature [21].

Various generalized integrators such as Second Order Generalized Integrator (SOGI), SOGI-Quadrature (SOGI-Q) etc. algorithms are presented in [22-25] for solar PV grid interfaced three phase system. The SOGI and SOGI-Q algorithms have poor system performance under the presence of the DC offset, high harmonics, and variation in system frequency. The Improved Second Order Generalized Integrator- Frequency Locked Loop (ISOGI-FLL) control scheme has better DC offset filtering capabilities. The ISOGI-FLL based control scheme is very robust to estimate quadrature component of fundamental load current with better DC offset and harmonic rejection capabilities. The major contribution of this work is as follows.

- The ISOGI-FLL based control has good DC component and harmonics elimination abilities along with better steady-state and dynamic response with respect to conventional control algorithms.
- The proposed ISOGI-FLL based control technique accommodates feed-forward unit, which mitigates the fluctuations in the grid currents due to deviation in the loads and SPG [26]. The steepest descent algorithm is used in the VSC switching algorithm to generate reference DC link voltage to extract crest power from PV array to enhance solar power injection into the grid.
- The proposed ISOGI-FLL algorithm has better steady-state and dynamic performance, high accuracy, low oscillations in amplitude estimation, low computational burden and low complexity as compared to conventional algorithms.

Simulated results are achieved using MATLAB/Simulink for various operating scenarios such as unbalancing in load side network and variation of solar irradiations. To confirm the effectiveness of the control algorithm, tests are performed on a prototype, which is developed in the laboratory for different conditions like load unbalancing, variable solar insolation, PV-DSTATCOM (Photovoltaic-Distribution Static Compensator) mode and DSTATCOM-PV mode.

II. System Topology and Proposed Control Scheme

Fig. 1 shows the single stage, PV-VSC based system tied to a three phase grid. This system contains a ripple filter, three

This article has been accepted for publication in a future issue of this journal, but has not been fully edited. Content may change prior to final publication. Citation information: DOI 10.1109/TIA.2018.2869880, IEEE Transactions on Industry Applications

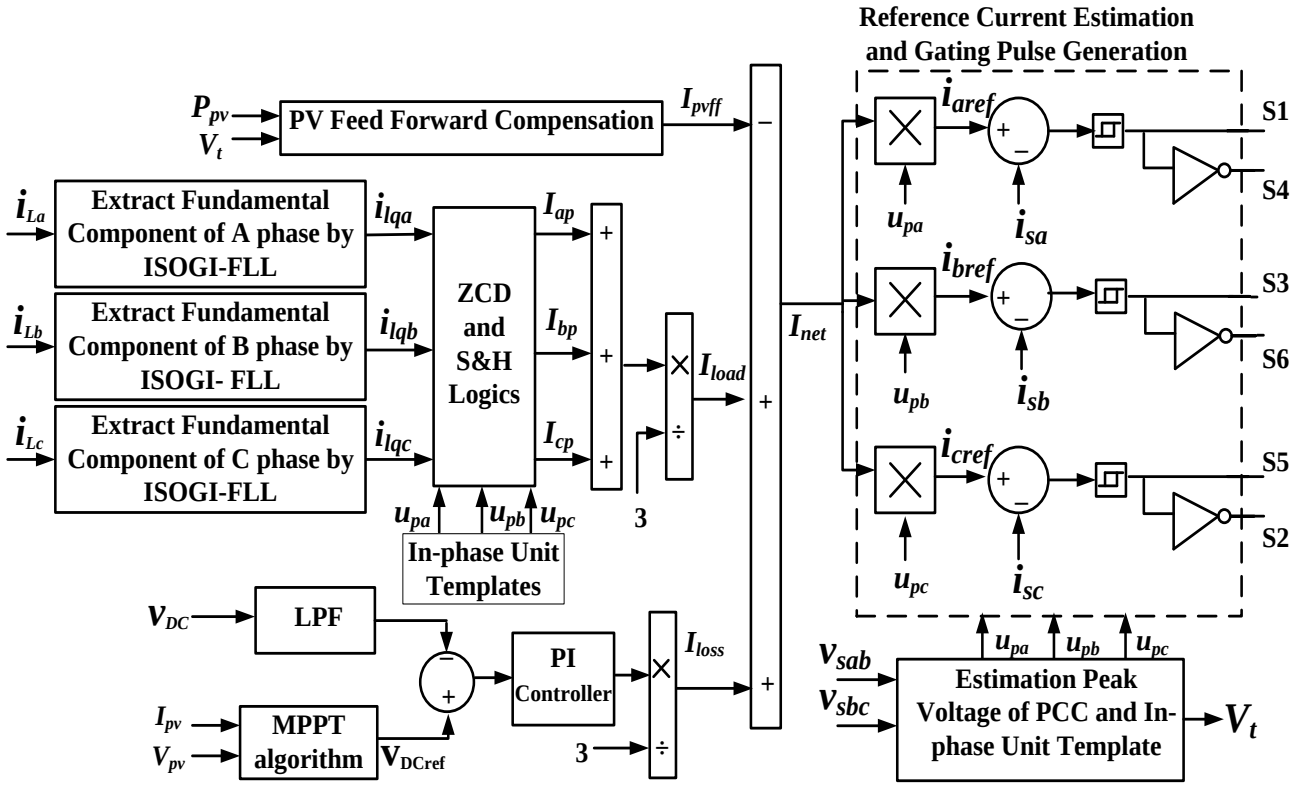

Fig. 2 Overall control structure of ISOGI-FLL based control algorithm.

phase grid, VSC, interfacing inductors, PV array and loads. The ripple filter is used to mitigate higher order harmonics produced due to switching ripple of the VSC. The interfacing inductor is used to reduce current harmonics in solar PV coupled VSC currents. The design procedure of this system is same as reported in the literature [9, 27].

The overall structure of ISOGI-FLL based control algorithm is depicted in Fig. 2. The steepest descent MPPT algorithm is used to operate PV array in such a way that the maximum power is delivered. The ISOGI-FLL technique is used to extract quadrature component of fundamental load current. The control algorithm includes MPPT control and switching control of VSC. The MPPT control is used to generate reference DC link voltage.

A. MPPT Control Approach

The steepest descent technique is used find Maximum Power Point (MPP). The main advantages of it, are that the steepest descent direction can be used with a different step size than the classical method that can substantially improve the convergence. The P&O algorithm has the major drawback of continuous oscillations in reference MPPT voltage. The same problem resembles in the incremental conductance algorithm, which is dissected in the steepest descent algorithm. The steepest descent algorithm shows better dynamic performance and smoother steady-state performance as compared to hill climbing method. It is also known as gradient descent method, which is originally an optimization method. The MPP is estimated as,

$$V_{DC}(k+1) = V_{DC}(k) + \frac{\left(dP_{pv}/dV_{DC}\right)_{V=V_{DC}(k)}}{k_{\varepsilon}} \tag{1}$$

where k_{ε} is step size corrector, decides how much steep in each step it takes in the gradient direction and it is around 7% to 10% of DC link voltage of VSC. The deviation of MPP in each step is indicated by (dp/dv). The value of dp/dv is calculated as,

$$\frac{dP_{pv}}{dV_{DC}} = f(V_{DC}(k), P_{pv}(k)) \tag{2}$$

$$\frac{dP_{pv}}{dV_{DC}} = \frac{P_{pv}(k+1) - P_{pv}(k)}{2(V_{DC}(k+1) - V_{DC}(k))} + O(\Delta V)^3 \tag{3}$$

where $O(\Delta V)^3$ is truncation error for center differentiation and second-order accuracy.

B. Switching Control Technique for VSC

The switching algorithm includes the estimation of the amplitude of PCC voltages, estimation of unit templates, loss component, a feed-forward unit of PV power and generation of the reference currents for the grid.

1) Estimation of Unit Templates

The phase voltages are calculated by sensing two line voltages (v_{sab} and v_{sbc}). The v_{sab} and v_{sbc} are passed through a band-pass filter to eliminate distortions. The phase voltages (v_{sa}, v_{sb}, and v_{sc}) are calculated as [27],

$$\begin{bmatrix} v_{sa} \\ v_{sb} \\ v_{sc} \end{bmatrix} = \frac{1}{3}\begin{bmatrix} 2 & 1 & 0 \\ -1 & 1 & 0 \\ -1 & -2 & 0 \end{bmatrix}\begin{bmatrix} v_{sab} \\ v_{sbc} \\ 0 \end{bmatrix} \tag{4}$$

This article has been accepted for publication in a future issue of this journal, but has not been fully edited. Content may change prior to final publication. Citation information: DOI 10.1109/TIA.2018.2869880, IEEE Transactions on Industry Applications

The typical value of PCC voltage (V_t) is computed as,

$$V_t = \sqrt{\frac{2}{3}\left(v_{sa}^2 + v_{sb}^2 + v_{sc}^2\right)} \tag{5}$$

Therefore, in-phase templates are estimated by dividing phase voltages by amplitude of terminal voltage (V_t), respectively. These in-phase unit templates are estimated as,

$$u_{pa} = \frac{v_{sa}}{V_t},\ u_{pb} = \frac{v_{sb}}{V_t},\ u_{pc} = \frac{v_{sc}}{V_t} \tag{6}$$

2) PV Feed Forward Term and Loss Component

The PV feed-forward term is used in the control scheme for variation in SPG and terminal voltage. From computed PV power and PCC voltage, PV feed-forward unit is evaluated as,

$$I_{pvff} = \frac{2P_{pv}}{3V_t} \tag{7}$$

The loss component (I_{loss}) is obtained from a Proportional Integral (PI) controller, which has the input of mismatch signal between V_{DCref} and V_{DC}. The loss component is evaluated as,

$$I_{loss} = (\mathrm{k}_P + \frac{k_I}{s})(V_{DCref} - V_{DC}) \tag{8}$$

3) Amplitude Estimation of Fundamental Load Current

The structure of ISOGI-FLL is depicted in Fig. 3. The modified SOGI and frequency locked loop, are two blocks, which are contained in ISOGI-FLL. The FLL controller estimates the frequency of the grid by using in-phase component (i_{ld}) and a quadrature component (i_{lq}). The input current i_L (with DC offset of 'A' and amplitude I_{pa}) then its transfer function is represented as,

$$I_L(\mathrm{s}) = \frac{I_{ap}\omega'}{s^2 + \omega'^2} + \frac{A}{s} \tag{9}$$

From Fig. 3, the transfer functions of in-phase gain (I_{ld})and quadrature phase gain (I_{lq}), are presented as,

$$I_{ld}(\mathrm{s}) = \frac{k\omega'\mathrm{s}}{s^2 + k\omega'\mathrm{s} + \omega'^2} I_L(\mathrm{s}) \tag{10}$$

$$I_{lq}(\mathrm{s}) = \frac{k\,\mathrm{s}^2}{s^2 + k\omega'\mathrm{s} + \omega'^2} I_L(\mathrm{s}) \tag{11}$$

The dynamic response of the in-phase and quadrature components of the generalized integrator is analyzed by considering the DC component in the load side network. Therefore, the in-phase and quadrature fundamental load components are obtained as,

$$I_{ld}(\mathrm{s}) = \frac{k\omega'\mathrm{s}}{\mathrm{s}^2 + k\omega'\mathrm{s} + \omega'^2}\left(I_{ap}\frac{\omega'}{s^2 + \omega'^2} + \frac{A}{s}\right) \tag{12}$$

$$I_{ld}(\mathrm{s}) = I_{ap}\frac{\omega'}{s^2 + \omega'^2} + \frac{(\mathrm{k}\,A - I_{ap})}{s^2 + k\omega'\mathrm{s} + \omega'^2} \tag{13}$$

The quadrature and in-phase components of fundamental current are represented as,

$$I_{lq}(\mathrm{s}) = \frac{k\,\mathrm{s}^2}{s^2 + k\omega'\mathrm{s} + \omega'^2}\left(I_{ap}\frac{\omega'}{s^2 + \omega'^2} + \frac{A}{s}\right) \tag{14}$$

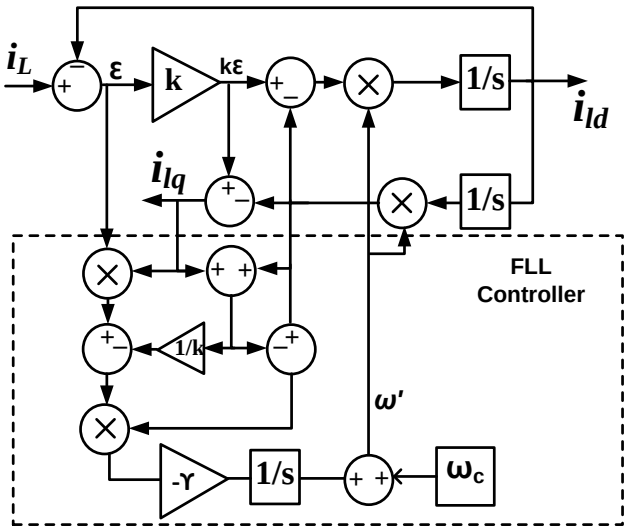

Fig. 3 Structure of ISOGI-FLL

$$I_{lq}(\mathrm{s}) = \frac{I_{ap}s}{s^2 + \omega'^2} + \frac{(\mathrm{k}\,A - I_{ap})\mathrm{s}}{\mathrm{s}(s^2 + k\omega'\mathrm{s} + \omega'^2)} \tag{15}$$

The fundamental load components (I_{ld} and I_{lq}) are converted into time domain as,

$$i_{ld}(\mathrm{t}) = I_{ap}\sin(\omega' t) + \frac{(\mathrm{k}\,A - I_{ap})}{\sqrt{1-\left(\frac{\mathrm{k}}{2}\right)^2}} e^{\frac{-\mathrm{k}\omega' t}{2}} \sin(\omega'\mathrm{t}\sqrt{1-\left(\frac{\mathrm{k}}{2}\right)^2}) \tag{16}$$

$$i_{lq}(\mathrm{t}) = I_{ap}\cos(\omega' t) - \frac{(\mathrm{k}\,A - I_{ap})}{\sqrt{1-\left(\frac{\mathrm{k}}{2}\right)^2}} e^{\frac{-\mathrm{k}\omega' t}{2}} \sin(\omega'\mathrm{t}\sqrt{1-\left(\frac{\mathrm{k}}{2}\right)^2} + \cos^{-1}(\mathrm{k}/2)) \tag{17}$$

From these equations of i_{ld} and i_{lq}, fundamental load terms are obtained as shown in Fig. 3. The in-phase fundamental load component has no any adverse effect on the performance of the control algorithm under the presence of the DC offset in steady state condition. The quadrature component (i_{lq}) is orthogonal to load current. For FLL controller, it has used a quadrature component (i_{lq}) of the fundamental load component and error (between the load current and in-phase component, i_{ld}) for estimation of the grid frequency. Moreover, FLL performance is not affected under the presence of the DC offset in load component in steady-state operating condition. Therefore, frequency adaptive structure of ISOGI-FLL is effective and robust to estimate the frequency of the grid. The amplitudes of fundamental load currents for three phases (I_{ap}, $I_{bp,}$ and I_{cp}) are estimated by zero crossing detectors, unit templates, sample and hold logics for respective phases. The net load component (I_{load}) of load currents, is obtained as,

$$I_{load} = \frac{I_{ap} + I_{bp} + I_{cp}}{3} \tag{18}$$

The net weight of the reference grid current is obtained using feed-forward, load and loss component. The total weight of reference grid current is evaluated as,

$$I_{net} = I_{load} - I_{pvff} + I_{loss} \tag{19}$$

This article has been accepted for publication in a future issue of this journal, but has not been fully edited. Content may change prior to final publication. Citation information: DOI 10.1109/TIA.2018.2869880, IEEE Transactions on Industry Applications

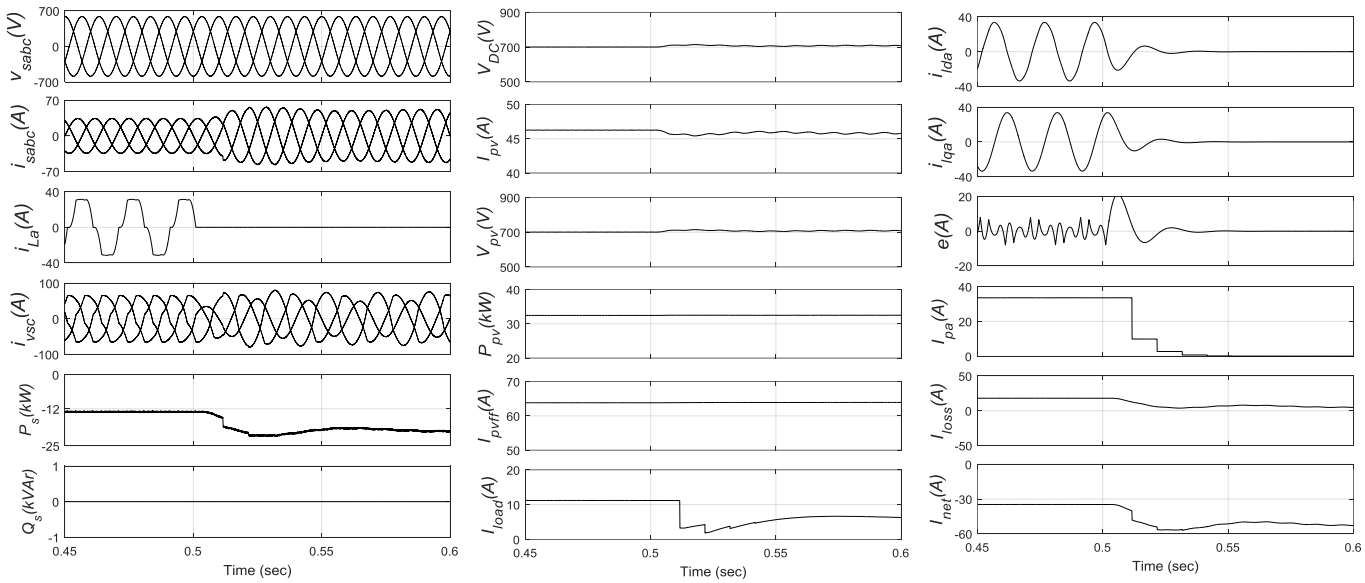

(a) (b) (c)

Fig. 4 Performance of the system under unbalancing in load side network (a) v_{sabc}, i_{sabc}, i_{La}, i_{vsc}, P_s, Q_s (b) V_{DC}, I_{pv}, V_{pv}, P_{pv}, I_{pvff}, I_{load} (c) i_{lda}, i_{lqa}, e, I_{pa}, I_{loss}, I_{net}

4) Reference Currents Estimation

The reference currents for the grid (i_{aref}, i_{bref} and i_{cref}), are obtained by multiplying net current component with unit templates (u_{pa}, u_{pb} and u_{pc}), respectively and are estimated as,

$$i_{aref} = u_{pa} * I_{net} \tag{20}$$

$$i_{bref} = u_{pb} * I_{net} \tag{21}$$

$$i_{cref} = u_{pc} * I_{net} \tag{22}$$

The current error is generated using reference and sensed grid currents, which is fed to the hysteresis current controller for switching pulses of the VSC.

III. Simulation Results

A 3-phase grid-tied SECS is modeled in MATLAB/Simulink using simpower system toolbox. The system performance is analyzed for unbalancing in load side network and variation in solar irradiation. The response of the system is demonstrated using signals such as grid voltages (v_{sabc}), grid currents (i_{sabc}), load current (i_{La}), VSC currents (i_{vsc}), grid powers (P_s, Q_s), solar PV array voltage-current-power (V_{pv}, I_{pv}, and P_{pv}), feed-forward term (I_{pvff}), loss term (I_{loss}), total magnitude component (I_{net}), load term (I_{load}) and DC link voltage (V_{DC}).

A. Dynamic Performance of the SECS

Figs. 4 (a-c) demonstrate the waveforms of the grid voltages (v_{sabc}), grid currents (i_{sabc}), load current (i_{La}), VSC currents (i_{vsc}), active-reactive powers in the grid (P_s,Q_s). As imbalancing manifests in load network, dynamics in v_{sabc} and i_{sabc} are illustrated in Fig. 4 (a). The magnitude of the grid currents are increased as power consumption in load, is decreased. As unbalancing occurs at 0.5 s, the load current in 'a' phase is reduced to zero. Therefore, the power delivered in load side network is reduced. Hence, the surplus power is supplied in the distribution grid, which is illustrated as the observable increment in active power in the distribution grid. The reactive power requirement is met by PV connected VSC at coupling point to meet the requirement of the local loads. The power factor of the grid is unity as demonstrated in Fig. 4(a). The VSC currents have lower order harmonics as depicted in Fig. 4(a). The PV-VSC provides the compensating currents at PCC as required by local loads. The required compensating currents consumed by the nonlinear loads, are provided by solar PV coupled VSC and it has made grid currents balanced and sinusoidal. Fig. 4(b) shows the waveforms of V_{DC}, I_{pv}, V_{pv}, P_{pv}, I_{pvff}, I_{load}. The V_{DC} is properly sustained to reference value even under unbalanced load as illustrated in Fig. 4(b). The I_{pv} and P_{pv} are maintained unaltered as illustrated in Fig. 4(b). The feed-forward unit is unaltered under load unbalancing as illustrated in Fig. 4(b). The load component is diminished as the amplitude of the phase 'a' is decreased to zero under unbalancing scenario as depicted in Fig. 4 (b).

Fig. 4(c) shows the intermediate signals of the control algorithm. It shows the dynamics of the in-phase component and quadrature component (i_{lad} and i_{laq}), error, the amplitude of the fundamental component (I_{pa}), loss component (I_{loss}) and net weight of current component (I_{net}). The i_{ld} and i_{lq} components are diminished as demonstrated in Fig. 4(c). The error and magnitude of fundamental component, are diminished to zero as a load of phase 'a' is opened. The total magnitude of the reference currents, is raised as load component reduces, which is illustrated in Fig. 4(c).

B. System Performance at Variation of Solar Insolation

Fig. 5(a) shows the performance of the system as solar insolation varied from 800W/m^2 to 1000W/m^2. Fig. 5(a) depicts the dynamics of the grid voltages-currents (v_{sabc}, i_{sabc}), load current (i_{La}), VSC currents (i_{vsc}), real and imaginary power in the grid (P_s and Q_s). The incremental change in magnitude of the grid currents are observed as SPG is increased. The dynamics of the load current is unaltered as illustrated in Fig. 5(a). The compensating currents with the active component, are supplied by solar PV-VSC as depicted in Fig. 5(a). The delivered real power in the grid is improved as SPG is increase-

This article has been accepted for publication in a future issue of this journal, but has not been fully edited. Content may change prior to final publication. Citation information: DOI 10.1109/TIA.2018.2869880, IEEE Transactions on Industry Applications

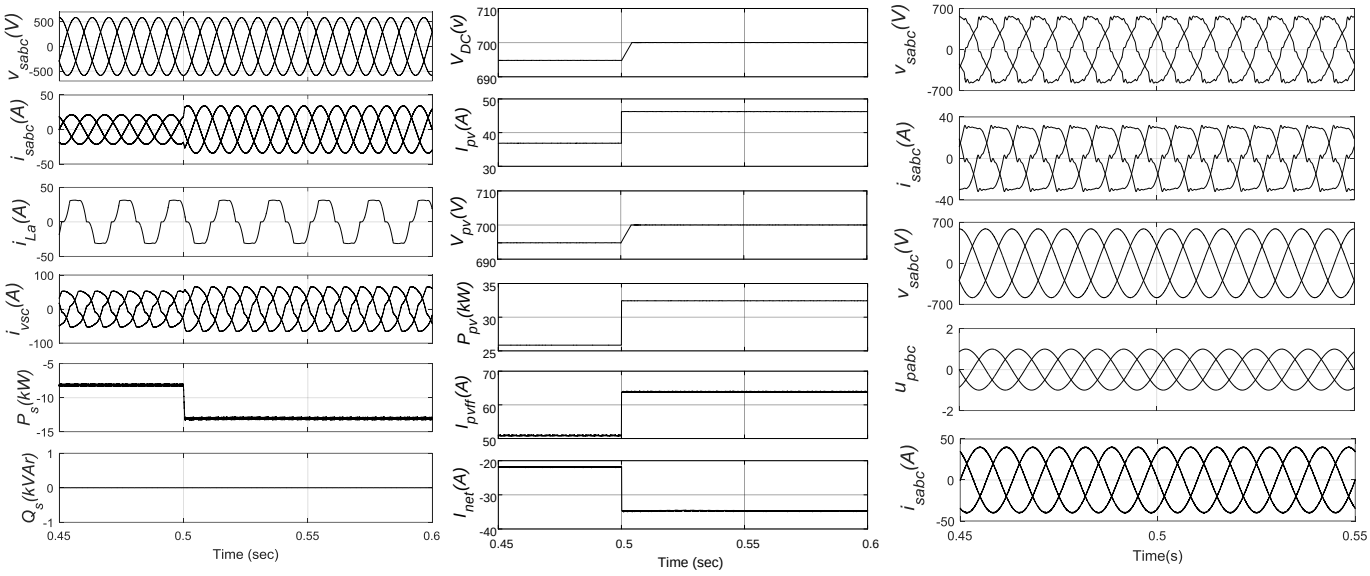

(a) (b)

Fig. 5 Performance of the system under (a-b) variation of solar insolation from800 W/m^2 to 1000 W/m^2, (a) v_{sabc}, i_{sabc}, i_{La}, i_{vsc}, P_s, Q_s (b) V_{DC}, I_{pv}, V_{pv}, P_{pv}, I_{pvff}, I_{net} (c) v_{sabc}, i_{sabc}, v_{sabc}, u_{pabc}, i_{sabc}

d. The Q_s in the grid is zero, which presents the unity power factor operation. Fig. 5(b) shows V_{DC}, I_{pv}, V_{pv}, P_{pv}, I_{pvff}, I_{net}. The V_{DC} is stable and regulated to new value under fluctuation of solar irradiations. The I_{pv} and P_{pv} are increased as illustrated in Fig. 5(b). The V_{PV} is followed according to DC bus voltage under variation of the solar irradiations. The PV feed-forward unit is raised as SPG increases. The net amplitude of the reference current is raised as the PV feed-forward term is increased.

C. *Performance of SECS under Distorted Grid Voltages*

Fig. 5 (c) shows the performance of the system under distorted grid voltages. When highly nonlinear loads are tied at the coupling point, the v_{sabc} contain distortion under weak grid [21]. Fig. 5(c) shows the waveforms of v_{sabc}, i_{sabc}, v_{sabc}, u_{pabc}, i_{sabc}. When solar PV-VSC is not connected at PCC, the dynamics of v_{sabc} and i_{sabc} are depicted in first two waveforms of Fig. 5(c) under distorted grid scenario. The grid currents are same as load currents when solar PV coupled VSC is connected at PCC. Therefore, PCC voltages are distorted due to immensely nonlinear local loads are connected at PCC. Third waveforms onward in Fig. 5(c) depict the performance of the system (v_{sabc}, u_{pabc}, i_{sabc}), when solar PV array coupled VSC is connected at PCC. When solar PV array coupled VSC is connected at PCC, it provides active power with harmonics compensation. Moreover, sensed PCC voltages are passed through the band-pass filter (BPF) to mitigate distortion in sensed line voltages. Therefore, unit templates are smooth as depicted in Fig. 5 (c). Hence, grid currents follow the smooth reference currents, which are depicted in Fig. 5(c). The THDs of PCC voltages are improved, which is observable in Fig. 5(c).

D. *Comparative Performance Between Various Algorithms*

The improved SOGI-FLL has good frequency tracking capability due to better DC offset rejection from the nonlinear load current. Fig. 6 shows the comparative performance of

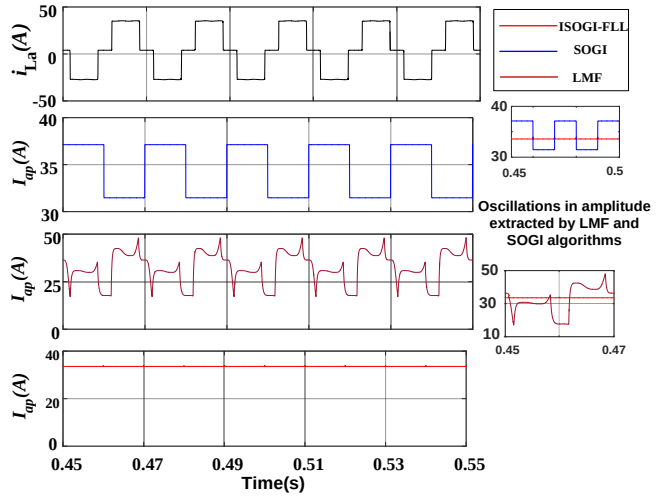

Fig. 6 Comparative performance between proposed algorithm with SOGI and LMF algorithms

proposed control algorithm with conventional control algorithms. The performance of conventional SOGI is affected by the presence of the DC offset (of 4 A considered here for comparative performance). However, the ISOFI-FLL control provides a good response as compared to conventional control [18-19] as shown in Fig. 6. There are noticeable oscillations in the output of the LMF and SOGI algorithms as shown in zoom view of comparative performance. The LMF algorithm has high fluctuations in the evaluated magnitude of the fundamental component due to 4th order optimization approach. Therefore, the performance of the system is affected using conventional algorithms under the presence of the DC offset in the load currents. It is easy to analyze that proposed control algorithm has better accuracy, high DSP speed, no oscillations in the extracted amplitude of the load component, low computational burden, low memory requirement.

This article has been accepted for publication in a future issue of this journal, but has not been fully edited. Content may change prior to final publication. Citation information: DOI 10.1109/TIA.2018.2869880, IEEE Transactions on Industry Applications

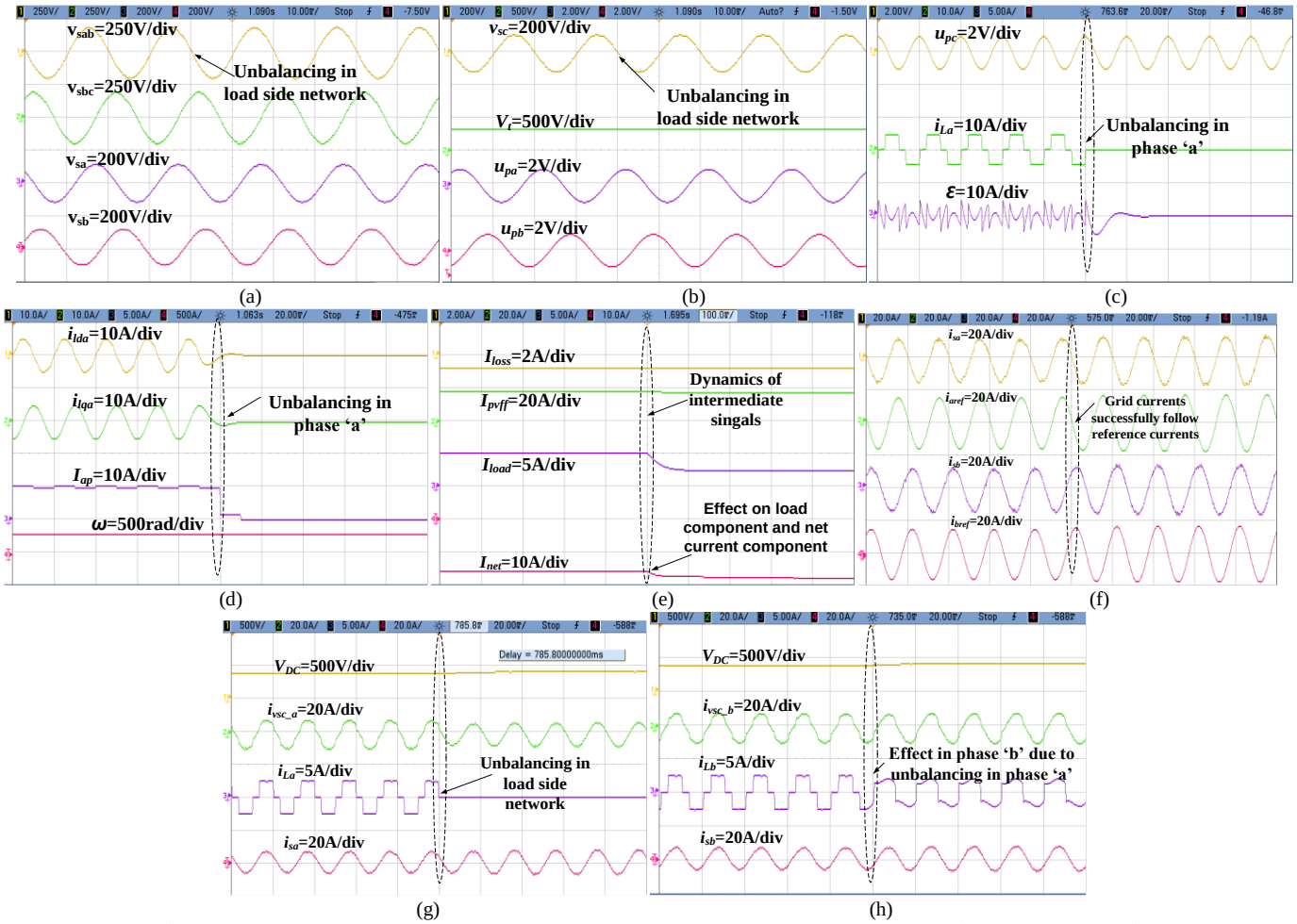

Fig. 7 Dynamics of system under unbalancing condition (a) v_{sab}, v_{sbc}, v_{sa}, v_{sb} (b) v_{sc}, V_t, u_a, u_b.(c) u_c, i_{la}, $\mathcal{E}$ (d) $i_{a'}$, $i_{aq'}$,i_{ap}, f (e) I_{loss}, I_{pvff}, i_{ap}, I_{net} (f) i_{sa}, i_{aref}, i_{sb}, i_{bref} (g) V_{DC}, i_{vsc_a}, i_{La}, i_{sa} (h) V_{DC}, i_{vsc_b}, i_{Lb}, i_{sb}

IV. EXPERIMENTAL RESULTS

A prototype of a three phase grid interfaced solar PV system is developed in the laboratory. The solar power simulator is utilized to implement solar-based power generation. The steady-state and dynamic responses of the system, are recorded using power analyzer (Fluke, make 43B) and a digital oscilloscope (AGILENT, make DSO-7014A), respectively. The proposed control scheme is implemented on a Digital Signal Processor (DSP) based on a MicroLab box dSAPCE-1102. The Hall-Effect voltage sensors (LV25-P) and current sensors (LA55-P) are used to sense two line voltages, PV array voltage, and grid currents, PV array current, load currents, respectively. To provide isolation between DSP signals and VSC, the optocouplers are used. The behaviour of the system is analyzed under variable solar irradiation levels, load unbalancing and various modes.

A. Dynamic Response under Load Unbalancing

Figs. 7 (a-h) depict the response of the system during unbalanced load scenario. The dynamics of the system is analyzed under load unbalancing of phase 'a'. Fig. 7 (a) shows dynamics of line voltages (v_{sab}, v_{sbc}) and phase voltages (v_{sa}, v_{sb}). The line and phase voltages are unaffected under load unbalancing. Fig. 7 (b) depicts the response of phase voltage (v_{sc}), the typical value of terminal voltage (V_t), unit-templates (u_{pa} and u_{pb}) during unbalancing condition. As there is no variation in phase voltages, the unit templates are unaffected under load unbalancing. Fig. 7 (c) shows unit template (u_{pc}), load current (i_{La}) and error (ε). The load current of phase 'a' is reduced to zero as demonstrated in Fig. 7 (c). The error, intermediate signals of the control algorithm, are diminished to zero as the unbalanced load occurs. Fig. 7 (d) shows in-phase and quadrature components of load current (i_{lda} and i_{lqa}), the amplitude of fundamental load current (I_{ap}) and frequency (ω) during unbalancing of load side network. The i_{lda} and i_{lqa} of the phase 'a', are diminished to zero as current approaches to zero. The magnitude of fundamental component is immediately diminished in a couple of cycles. Fig. 7 (e) presents dynamics of loss component (I_{loss}), PV feed-forward component (I_{pvff}), load component (I_{load}) and total weight (I_{net}) during unbalancing of phase 'a'. The loss component is unaltered even under fluctuations of the load. The loss component and PV feed-forward unit, remain unaltered even under a variation of the load side network. The load component is reduced as unbalancing occurs in local loads. The net magnitude of the reference currents are shown in Fig. 7 (f). The grid currents (i_{sa}, i_{sb}) and reference currents (i_{aref}, i_{bref}), are shown in Fig. 7 (f). The reference grid currents are increased as load unbalancing occurs due to delivered power in load side network is reduced. The grid currents have effectively tracked reference grid curr-

This article has been accepted for publication in a future issue of this journal, but has not been fully edited. Content may change prior to final publication. Citation information: DOI 10.1109/TIA.2018.2869880, IEEE Transactions on Industry Applications

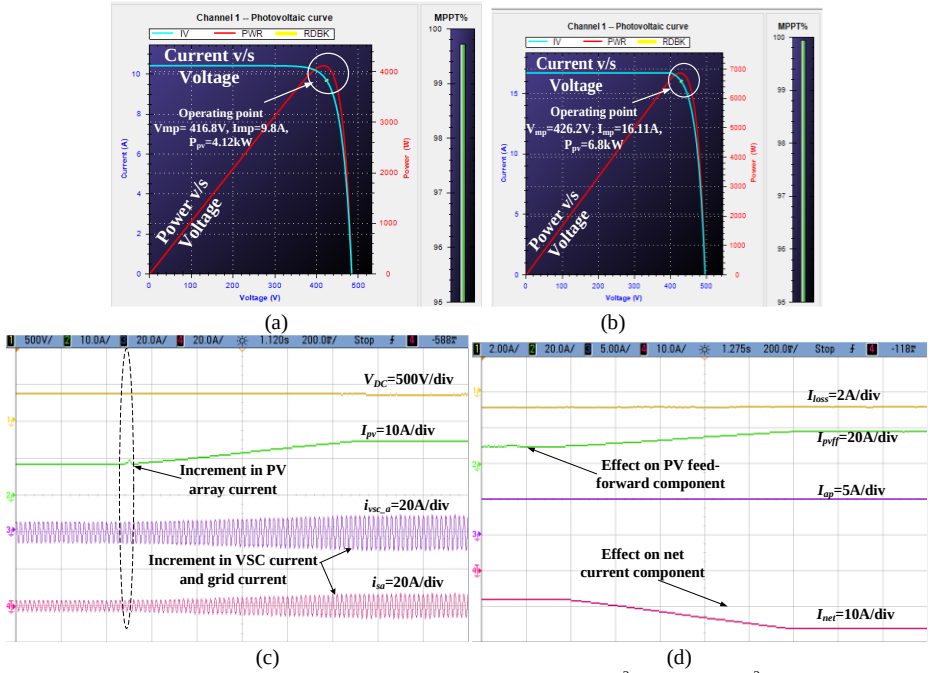

Fig. 8 The operating point PV simulator and MPPT at variable insolation level (a) 600 W/m^2 (b) 1000 W/m^2 (c) V_{DC}, I_{pv}, i_{vsc_a}, i_{sa} (d) I_{loss}, I_{pvff}, I_{ap}, I_{net}

ents. Fig. 7 (g) shows response of DC link voltage (V_{DC}), VSC current (i_{vsc_a}), load current (i_{La}) and source current (i_{sa}). The DC link voltage is settled to a new value corresponding to MPPT during a dynamic condition of the presented system, while grid currents are increased and these remain sinusoidal and balanced. Fig. 7 (h) shows the effect of load unbalancing on phase 'b' due to phase 'a' and waveforms of V_{DC}, VSC current (i_{vsc_b}), load current (i_{lb}) and grid current (i_{sb}). The i_{sb} is maintained sinusoidal as shown in Fig. 7 (h).

B. System Response under Varying Insolations

The response of a grid connected SECS is analyzed in Figs. 8(a-d) under deviation of the insolation from 600 W/m^2 to 1000 W/m^2. Figs. 8 (a-b) present the response of the MPPT algorithm for solar PV array simulator at different solar insolation levels. Fig. 8 (c) demonstrates the dynamics of V_{DC}, I_{pv}, i_{vsc_a}, and i_{sa}. The V_{DC} is sustained stable at new value under deviation of SPG as demonstrated in Fig. 8 (c). The I_{pv} rises as solar irradiation is increased. Therefore, the active power in the distribution grid is raised, which is illustrated by the incremental change in amplitude of grid current as illustrated in Fig. 8 (c). Fig. 8 (d) presents loss component (I_{loss}), PV feed-forward component (I_{pvff}), load component (I_{ap}) and total weight (I_{net}). The feed-forward unit is raised as the solar irradiation is raised. The net amplitude of reference current is raised due to observable change in PV feed-forward unit as illustrated in Fig. 8 (d).

C. Steady-state Performance of SECS

The steady-state behaviour of presented SECS is shown in Figs. 9 (a-c). Figs. 9 (a-b-c) present waveforms of voltage-current of the grid, load, and VSC, respectively. Figs. 9 (d-f) show the power of grid, load, and PV-VSC. The solar PV-VSC provides real power to the local load and remaining of power is delivered to the grid as depicted in Figs. 9 (d-f). Figs. 9 (g-i) show harmonic spectra of the i_{sa}, i_{La}, and v_{sab}. The THD of the i_{La} is more than limit according to the IEEE-519 standard [28].

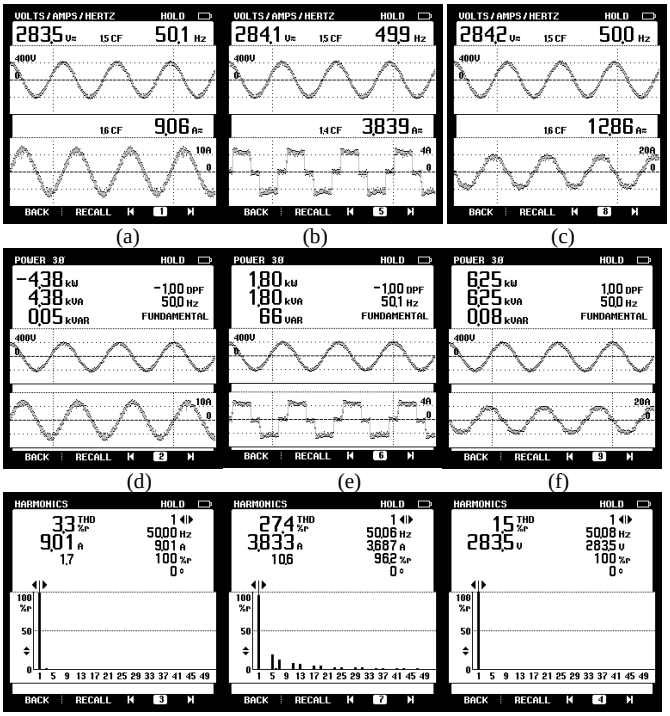

Fig. 9 Steady-state behaviour of the SECS (a-c) v_{sab}-i_{sa}, v_{sab}-i_{La}, v_{sab}-i_{vsca} (d-f) power in grid-load-solar PV-VSC power (g-i) harmonic spectrum of i_{sa}, i_{la}, and v_{sab}

However, the THD of the i_{sa} is achieved within limit according to the IEEE-519 standard [28]. Moreover, the grid voltage and currents are achieved within the restriction of the IEEE-519 standard [28].

D. PV Mode to DSTATCOM Mode

When the SPG is reduced to zero then the behavior of SECS is transited from PV mode to DSTATCOM mode. To maintain DC bus voltage at the maximum power point, PCC coupled VSC draws active power from the grid, which is accounted as

This article has been accepted for publication in a future issue of this journal, but has not been fully edited. Content may change prior to final publication. Citation information: DOI 10.1109/TIA.2018.2869880, IEEE Transactions on Industry Applications

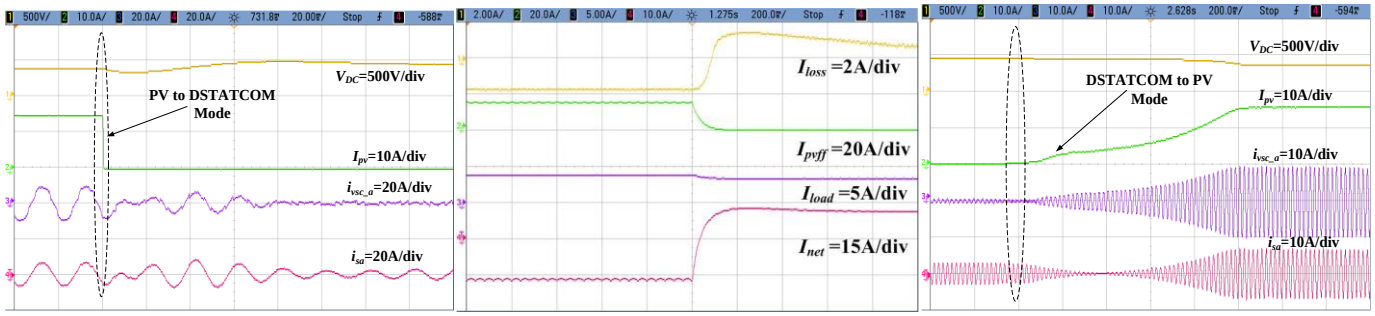

(a) (b)

Fig. 10 Response of SECS under (a-b) PV to DSTATCOM mode, V_{DC}, I_{pv}, i_{vsc_a}, i_{sa} (b) I_{loss}, I_{pvff}, I_{load} I_{net} (c) DSTATCOM to PV mode, V_{DC}, I_{pv}, i_{vsc_a}, i_{sa}

an active loss. Therefore, a loss component is included into the control scheme to accommodate losses in the VSC. The minute variation in loss component is observable to regulate V_{DC}. The waveforms of V_{DC}, I_{pv}, $i_{vsc\_a,}$ and i_{sa} are shown in Fig. 10 (a). The V_{DC} is maintained stable in DSATATCOM mode. In DSTATCOM mode, the real and reactive power are supplied to the local loads by the grid and VSC, respectively as depicted in Fig. 10 (a). Fig. 10 (b) demonstrates the I_{loss}, I_{pvff}, $I_{load,}$ and I_{net}. The loss component varies as SECS changes from PV mode to DSTATCOM mode. The feed-forward term is reduced to zero as solar power generation becomes zero. The load component is not much affected while the transition to DSTATCOM mode. The net component of reference grid currents, is affected according to variation in the feed-forward component.

E. DSTATCOM to PV Mode

When the solar power generation is recovered then the system behavior is transited from to DSTATCOM mode to PV mode. Fig. 10 (c) shows waveforms of V_{DC}, I_{pv}, i_{vsc_a} and i_{sa}. The solar PV coupled VSC consumes power from PCC to regulate DC bus voltage. In PV mode, solar PV-VSC provides real power to the load and surplus of power transfer to the grid. The PV-VSC provides compensating currents at coupling point to enhance the power factor of the grid.

V. CONCLUSION

The proposed single stage PV system interfaced to the grid with an ISOGI-FLL based control algorithm, has been found quite robust and suitable for various conditions by improving PQ of the distribution network like load balancing, power factor correction, and harmonics elimination while supplying the active power to the grid. The steepest descent MPPT technique has extracted efficiently maximum power from PV array and it has maintained DC link voltage to desired value effectively. The ISOGI-FLL based structure has increased an accuracy of a control algorithm for the presented system by extraction of the quadrature component of fundamental load current effectively. The ISOGI-FLL based control has been verified experimentally on a developed prototype in the laboratory and obtained responses have been found satisfactory. The THD of grid current has been found well within limit according to an IEEE-519 standard.

APPENDENCES

A. Simulation Parameters

Grid voltage, v_{sab}= 415 V; DC bus capacitor, C_{DC}= 6 mF; Solar PV array details: V_{mpp}= 710 V, I_{mpp}= 45 A, P_{pv}= 32.5 kW;. K_p= 4.8; K_i= 1; DC bus voltage, V_{DC}= 710 V; interfacing inductor, L_f= 2.5 mH; sampling time, nonlinear load, R= 25 Ω, L= 80 mH; T_s= 10 μs; ripple filter: R_f= 5Ω, C_f= 10 μF.

B. Experimental Parameters

Solar PV array simulator V_{mp} = 426.2V, I_{mp}=16.11 A, P_{pv} = 6.8 kW; DC link voltage = 426.2 V; grid voltage v_{sab} = 285 V, 50 Hz; VSC rating = 25 kVA; Interfacing inductor L_f = 3mH; ripple filter R_f= 18Ω and C_f = 10μF; ϒ = -46; ω_c = 314; non-linear load = 1.8 kVA; K_p = 0.13; K_i = 0.002; sampling time = 30μs.

REFERENCES

[1] S. S. Chandel, R. Shrivastva, V. Sharma and P. Ramasamy, "Overview of the initiatives in renewable energy sector under the national action plan on climate change in India," *Renewable and Sustainable Energy Reviews*, vol. 54, pp. 866-873. Feb. 2016.

[2] IEA, *Renewable Energy: Medium-term Market Report*. International Energy Agency. 2012.

[3] D. S. Shugar and S. Ramon, "Photovoltaic in the utility distribution system: the evaluation of system and distributed benefits," in *Proc. IEEE Photovoltaic Specialist Conference*, vol. 2, pp. 836-843, 21-25 May, 1990.

[4] A. K. Barnes, J. C. Balda and C. M. Stewart, "Selection of converter topologies for distributed energy resources," in *Proc. IEEE Applied Power Electronics Conference and Exposition (APEC)*, pp. 1418-1423, 2012.

[5] T. F. Wu, C. H. Chang, L. C. Lin and C. L. Kuo, "Power loss comparison of single- and two-stage grid-connected photovoltaic systems," *IEEE Transactions Energy Conversion*, vol. 26, no. 2, pp. 707-715, 2011.

[6] A. S. O. Ogunjuyigbe, T. R. Ayodele, V. E. Idika and O. Ojo, "Effect of lamp technologies on the power quality of electrical distribution network," in *Proc. IEEE Power Energy System*, pp. 159-163, 2017.

[7] X. Liang, "Emerging power quality challenges due to integration of renewable energy sources," *IEEE Transactions Industry Applications*, vol. 53, no. 2, pp. 855-866, March-April 2017.

[8] A. Javadi, A. Hamadi and K. Al-Haddad, "Three-phase power quality device tor weak Systems based on SRF and p-q theory controller," in *Proc. IEEE Industrial Electronics Society*, pp. 345-350, 2015.

[9] R. K. Agarwal, I. Hussain and B. Singh, "LMF-based control algorithm for single stage three-phase grid integrated solar PV system," *IEEE Transactions Sustainable Energy*, vol. 7, no. 4, pp. 1379-1387, Oct. 2016.

[10] L. Tarisciotti, "Model predictive control for shunt active filters with fixed switching frequency," *IEEE Transactions Industry Applications*, vol. 53, no. 1, pp. 296-304, Jan.-Feb. 2017.

[11] B. Singh, C. Jain, S. Goel, A. Chandra and K. Al-Haddad, "A multifunctional grid-tied solar energy conversion system with ANF-based control approach," *IEEE Transactions Industry Applications*, vol. 52, no. 5, pp. 3663-3672, 2016.

[12] S. W. Kang and K. H. Kim, "Sliding mode harmonic compensation strategy for power quality improvement of a grid-connected inverter under

distorted grid condition," *IET Power Electronics*, vol. 8, no. 8, pp. 1461-1472, 2015.

[13] R. Panigrahi and B. Subudhi, "Performance enhancement of shunt active power filter using a Kalman filter-based H-infinity control strategy," *IEEE Transactions Power Electronics*, vol. 32, no. 4, pp. 2622-2630, April 2017.

[14] I. Kamwa and R. Grondin, "Fast adaptive schemes for tracking voltage phasor and local frequency in power transmission and distribution systems," *IEEE Transactions Power Delivery*, vol. 7, no. 2, pp. 789-795, Apr 1992.

[15] D. S. Ochs, B. Mirafzal and P. Sotoodeh, "A method of seamless transitions between grid-tied and stand-alone modes of operation for utility-interactive three-phase inverters," *IEEE Transactions Industry Applications*, vol. 50, no. 3, pp. 1934-1941, May-June 2014.

[16] N. Sung, J. Lee, B. Kim, M. Park, and I.-K. Yu, "Novel concept of a PV power generation system adding the function of shunt active filter," in *Proc. IEEE/PES Trans. Distrib. Conf. Exhib*, vol. 3, 2002, pp. 1658–1663.

[17] B. Singh, P. Jayaprakash, S. Kumar and D. P. Kothari, "Implementation of neural-network-controlled three-leg VSC and a transformer as three-phase four-wire DSTATCOM," *IEEE Transactions Industry Applications*, vol. 47, no. 4, pp. 1892-1901, 2011.

[18] M. Qasim and V. Khadkikar, "Application of artificial neural networks for shunt active power filter control," *IEEE Transactions Industrial Informatics*, vol. 10, no. 3, pp. 1765-1774, Aug. 2014.

[19] T. Penthia, A. K. Panda, S. K. Sarangi and M. Mangaraj, "ADALINE based LMS algorithm in a three phase four wire distribution system for power quality enhancement," in *Proc. IEEE 6th International Conference on Power Systems (ICPS)*, pp. 1-5, 2016.

[20] P. Shah, I. Hussain and B. Singh, "Real-time implementation of optimal operation of single-stage grid interfaced PV system under weak grid conditions" *IET Generation Transmission and Distribution*, Early Access.

[21] A. Adib, B. Mirafzal, X. Wang and F. Blaabjerg, "On stability of voltage source inverters in weak grids," *IEEE Access*, vol. 6, pp. 4427-4439, 2018.

[22] S. Kumar, I. Hussain, B. Singh, A. Chandra and K. Al Haddad, "An adaptive control scheme of SPV system integrated to three phase AC distribution system," *IEEE Transactions Industry Applications*, vol. 53, no. 6, pp. 5173-5181, 2017.

[23] C. Jain and B. Singh, "A SOGI-FLL based control algorithm for single phase grid interfaced multifunctional SPV under non ideal distribution system," in *Proc. IEEE India Conference (INDICON)*, Pune, pp. 1-6, 2014.

[24] P. Shah. I. Hussain and B. Singh, "Single stage SECS interfaced with grid using ISOGI-FLL based control algorithm" in *Proc. IEEE India International Conf. Power Electronics (IICPE)*, pp. 1-6, 2016.

[25] P. Shah, I. Hussain and B. Singh, "Multi-resonant FLL based control algorithm for grid interfaced multi-functional solar energy conversion" *IET Science, Measurement & Technology*, vol. 12, no. 1, pp. 49-62, 2018.

[26] A. Luo, Y. Chen, Z. Shuai and C. Tu, "An improved reactive current detection and power control method for single-phase photovoltaic grid-connected DG system," *IEEE Transactions Energy Conversion*, vol. 28, no. 4, pp. 823-831, Dec. 2013.

[27] B. Singh, A. Chandra and K. Al-Haddad, *Power quality: problems and mitigation techniques*, John Wiley & Sons Ltd., United Kingdom, 2015.

[28] IEEE Recommended Practice and Requirement for Harmonic Control on Electric Power System, IEEE std. 519, 2014.

Priyank Shah (M'16) was born in Vadodara, Gujarat, India, in 1992. He received his B. E in Electrical Engineering from Birla Vishvakarma Mahavidyalaya (BVM), Gujarat, India, in 2013. He joined for M.Tech degree in Indian Institute of Technology Delhi in 2015. He is currently pursing Ph. D degree in Indian Institute of Technology Delhi (IITD), New Delhi, India.

His areas of interest includes phase locked loop (PLL), applications of adaptive and learning control for renewable power generation, power quality improvement of the distributed network, virtual synchronous generator (VSG), fault ride through operation and synchronization and is-landing techniques.

Ikhlaq Hussain (M'14) was born in Doda, Jammu and Kashmir, India, in 1986. He received his B. E. (Electrical) from University of Jammu, Jammu, India, in 2009 and M. Tech. (Gold Medalist) in Electrical Power System Management from the Jamia Millia Islamia (A Central University), New Delhi, India, in 2012. He is currently working toward his Ph.D. in the Department of Electrical Engineering, Indian Institute of Technology Delhi, New Delhi, India.

From September 2012 to December 2012, he was a Lecturer with the Department of Electrical Engineering, National Institute of Technology Srinagar, India. On 19th April 2017, he joined as Assistant Professor in the Department of Electrical Engineering, Institute of Technology, University of Kashmir, Srinagar, India. His areas of research interests include power electronics, power quality, custom power devices, renewable energy systems, power system management and microgrid.

Mr. Hussain was a recipient of the POSOCO power system award (PPSA) from Power System Operation Corporation (POSOCO) Limited, India and Foundation for Innovation and Technology Transfer (FITT) at Indian Institute of Technology Delhi in 2017, and the IEEE INDICON Best Paper Award in 2015 and the IEEE UPCON Best Paper Award in 2016.

Bhim Singh (SM'99, F'10) was born in Rahamapur, Bijnor (UP), India, in 1956. He received his B.E. (Electrical) from University of Roorkee, India, in 1977 and his M.Tech. (Power Apparatus & Systems) and Ph.D. from Indian Institute of Technology Delhi, India, in 1979 and 1983, respectively.

In 1983, he joined the Department of Electrical Engineering, University of Roorkee (Now IIT Roorkee), as a Lecturer. He became a Reader there in 1988. In December 1990, he joined Department of Electrical Engineering, IIT Delhi, India, as an Assistant Professor, where he has become an Associate Professor in 1994 and a Professor in 1997. He has been ABB Chair Professor from September 2007 to September 2012. He has been Chair Professor from October 2012 to September 2017. He has been Head of the Department of Electrical Engineering at IIT Delhi from July 2014 to August 2016. Since, August 2016, he is the Dean, Academics at IIT Delhi. He is JC Bose Fellow of DST, Government of India since December 2015.

Prof. Singh has guided 68 Ph.D. Dissertations and 167 M.E./M.Tech./M.S.(R) theses. He has been filed 24 patents. He has executed more than eighty sponsored and consultancy projects. He has co-authored a text book on power quality: Power Quality Problems and Mitigation Techniques published by John Wiley & Sons Ltd. 2015.

His areas of interest include solar PV grid interfaced systems, microgrids, power quality monitoring and mitigation, solar PV water pumping systems, improved power quality AC-DC converters, power electronics, electrical machines, drives, renewable energy systems, FACTS, and high voltage direct current (HVDC) systems.

Prof. Singh is a Fellow of the Indian National Academy of Engineering (FNAE), The Indian National Science Academy (FNA), The National Academy of Science, India (FNASc), The Indian Academy of Sciences, India (FASc), The World Academy of Sciences (FTWAS), Institute of Electrical and Electronics Engineers (FIEEE), the Institute of Engineering and Technology (FIET), Institution of Engineers (India) (FIE), and Institution of Electronics and Telecommunication Engineers (FIETE) and a Life Member of the Indian Society for Technical Education (ISTE), System Society of India (SSI), and National Institution of Quality and Reliability (NIQR).

He has received Khosla Research Prize of University of Roorkee in the year 1991. He is recipient of JC Bose and Bimal K Bose awards of The Institution of Electronics and Telecommunication Engineers (IETE) for his contribution in the field of Power Electronics. He is also a recipient of Maharashtra State National Award of Indian Society for Technical Education (ISTE) in recognition of his outstanding research work in the area of Power Quality. He has received PES Delhi Chapter Outstanding Engineer Award for the year 2006. Professor Singh has received Khosla National Research Award of IIT Roorkee in the year 2013. He also received Shri Om Prakash Bhasin Award-2014 in the field of Engineering including Energy & Aerospace. He has received 2017 IEEE PES Nari Hingorani Custom Power Award.

This article has been accepted for publication in a future issue of this journal, but has not been fully edited. Content may change prior to final publication. Citation information: DOI 10.1109/TIA.2018.2869880, IEEE Transactions on Industry Applications

He has been the General Chair of the 2006 IEEE International Conference on Power Electronics, Drives and Energy Systems (PEDES'2006), General Co-Chair of the 2010 IEEE International Conference on Power Electronics, Drives and Energy Systems (PEDES'2010), General Co-Chair of the 2015 IEEE International Conference (INDICON'2015), General Co-Chair of 2016 IEEE International Conference (ICPS'2016) held in New Delhi.